Inorg. Chem. **2004**, *43*, 3647–3655

Terminal Ligand Influence on the Electronic Structure and Intrinsic Redox Properties of the $[Fe_4S_4]^{2+}$ Cubane Clusters

You-Jun Fu, Xin Yang, Xue-Bin Wang, and Lai-Sheng Wang*

W. R. Wiley Environmental Molecular Sciences Laboratory, Pacific Northwest National Laboratory, P.O. Box 999, Richland, Washington 99352, and Department of Physics, Washington State University, 2710 University Drive, Richland, Washington 99352

Received April 11, 2004

We used photoelectron spectroscopy (PES) to study how the terminal ligands influence the electronic structure and redox properties of the [4Fe-4S] cubane in several series of ligand-substituted analogue complexes: $[Fe_4S_4Cl_{4-x}(CN)_x]^{2-}$, $[Fe_4S_4Cl_{4-x}(SCN)_x]^{2-}$, $[Fe_4S_4Cl_{4-x}(OAc)_x]^{2-}$, $[Fe_4S_4(SC_2H_5)_{4-x}(OPr)_x]^{2-}$, and $[Fe_4S_4(SC_2H_5)_{4-x}Cl_x]^{2-}$ ($x = 0$–4). All the ligand-substituted complexes gave similar PES spectral features as the parents, suggesting that the mixed-ligand coordination does not perturb the electronic structure of the cubane core significantly. The terminal ligands, however, have profound effects on the electron binding energies of the cubane and induce significant shifts of the PES spectra, increasing in the order $SC_2H_5^- \rightarrow Cl^- \rightarrow OAc^-/OPr^- \rightarrow CN^- \rightarrow SCN^-$. A linear relationship between the electron binding energies and the substitution number x was observed for each series, indicating that each ligand contributes independently and additively to the total binding energy. The electron binding energies of the gaseous complexes represent their intrinsic oxidation energies; the observed linear dependence on x is consistent with similar observations on the redox potentials of mixed-ligand cubane complexes in solution. The current study reveals the electrostatic nature of the interaction between the [4Fe-4S] cubane core and its coordination environment and provides further evidence for the electronic and structural stability of the cubane core and its robustness as a structural and functional unit in Fe–S proteins.

1. Introduction

Iron−sulfur proteins are the most distributed proteins in nature and play critical roles in biological electron transfers, catalysts, and gene expression regulation.[1,2] The different types of Fe−S active sites are usually coordinated by S from cysteine residues. The most common Fe−S active site is the [4Fe-4S] cubane cluster, in which each Fe is coordinated by three inorganic S's in the cubane core and one terminal ligand from a cysteine side chain. Despite their structural similarity, the redox potentials of Fe−S proteins span a wide range.[3−5] Contributions to these variations have been classified to come from the intrinsic electronic structure of the cubane and extrinsic factors due to the protein environment.[3,6−8] Major environmental factors contributing to the reduction potentials have been suggested to include H-bonding to the cysteine and bridging sulfide ligands, dipole interactions with the Fe−S cluster from the solvent and the protein side chain/backbone, and other electrostatic interactions. Theoretical calculations of the reduction potential of the [4Fe-4S] cluster were carried out, in which environmental effects were evaluated using a continuum dielectric model.[7,8]

Understanding the intrinsic electronic structure of the active center and how they respond to the extrinsic factors

* Author to whom correspondence should be addressed at Washington State University. E-mail: ls.wang@pnl.gov.

(1) (a) Beinert, H.; Holm, R. H.; Munck, E. *Science* **1997**, *277*, 653−659. (b) Beinert, H. *J. Biol. Inorg. Chem.* **2000**, *5*, 2−15.
(2) Holm, R. H.; Kennepohl, P.; Solomon, E. I. *Chem. Rev.* **1996**, *96*, 2239−2314
(3) Stephens, P. J.; Jollie, D. R.; Warshel, A. *Chem. Rev.* **1996**, *96*, 2491−2513.
(4) (a) Agarwal, A.; Li, D.; Cowan, J. A. *J. Am. Chem. Soc.* **1996**, *118*, 927−928. (b) Mansy, S. S.; Xiong, Y.; Hemann, C.; Hille, R.; Sundaralingam, M.; Cowan, J. A. *Biochemistry* **2002**, *41*, 1195−1201.
(5) (a) Iismaa, S. E.; Vazquez, A. E.; Jensen, G. M.; Stephens, P. J.; Butt, J. N.; Armstrong, F. A.; Burgess, B. K. *J. Biol. Chem.* **1991**, *266*, 21563−21571. (b) Shen, B.; Jollie, D. R.; Diller, T. C.; Stout, C. D.; Stephens, P. J.; Burgess, B. K. *Proc. Natl. Acad. Sci. U.S.A.* **1995**, *92*, 10064−10068.
(6) (a) Beck, B. W.; Xie, Q.; Ichiye, T. *Biophys. J.* **2001**, *81*, 601−613. (b) Swartz, P. D.; Beck, B. W.; Ichiye, T. *Biophys. J.* **1996**, *71*, 2958−2969.
(7) (a) Torres, R. A.; Lovell, T.; Noodleman, L.; Case, D. A. *J. Am. Chem. Soc.* **2003**, *125*, 1923−1936. (b) Mouesca, J. M.; Chen, J. L.; Noodleman, L.; Bashford, D.; Case, D. A. *J. Am. Chem. Soc.* **1994**, *116*, 11898−11914.
(8) Mouesca, J.-M.; Lamotte, B. *Coord. Chem. Rev.* **1998**, 178−180, 1573−1614.

10.1021/ic0495261 CCC: $27.50
Published on Web 05/15/2004

are important to understand the functionality of the Fe−S proteins. Synthetic analogue complexes provide ideal model systems to probe the intrinsic electronic structures of the cubane complexes and how the electronic structures are influenced by the ligand environment or other extrinsic factors.[9] Various spectroscopic techniques and theoretical methods have been used to investigate the magnetic and electronic properties of both synthetic analogues and proteins.[11−15] Extensive broken symmetry density functional theory (DFT) calculation[7,8,10,16] showed that the $[Fe_4S_4]^{2+}$ core can be viewed as a two-layer system, where two high-spin Fe's in each [2Fe-2S] sublayer are coupled ferromagnetically and the two [2Fe-2S] sublayers are coupled antiferromagnetically to give a low-spin state. This is consistent with experimental observations from Mossbauer,[11,13] EPR spectroscopy,[12,14] and K-edge X-ray absorption spectroscopy.[15] In our previous works, using a combined technique of electrospray ionization mass spectrometry (ESI-MS) and photoelectron spectroscopy (PES),[17] we have observed symmetric fission[18] of $[Fe_4S_4]^{2+}$ into $[Fe_2S_2]^{+}$ and investigated the intrinsic electronic structures of several [4Fe-4S] cluster complexes.[19]

In the current article, we present an experimental investigation of the influence of the terminal ligands on the [4Fe-4S] cubane core in mixed ligand systems. PES spectra of several series of analogue complexes with mixed terminal ligands, $[Fe_4S_4Cl_{4-x}(CN)_x]^{2-}$, $[Fe_4S_4Cl_{4-x}(SCN)_x]^{2-}$, $[Fe_4S_4Cl_{4-x}(OAc)_x]^{2-}$, $[Fe_4S_4(SC_2H_5)_{4-x}Cl_x]^{2-}$, and $[Fe_4S_4(SC_2H_5)_{4-x}(OPr)_x]^{2-}$ ($x = 0-4$), were measured. It was discovered that all the mixed-ligand species gave similar PES spectral features, whereas their electron binding energies are very sensitive to the terminal ligand substitution. A linear relationship between the binding energy and the substitution number was observed for each series, suggesting each ligand contributes independently to the total binding energy. The implications of these observations toward the understanding of the electronic structure of the cubane core and the insight into the ligand−core interactions are discussed. We also compare the current observations with redox potentials of mixed-ligand cubanes in solution.

2. Experimental Methods

All sample preparations were carried out in a dry N_2 glovebox using O_2-free acetonitrile as solvent. The 1×10^{-3} mol/L solutions of $[Fe_4S_4Cl_4]^{2-}$ (**1**) and $[Fe_4S_4(SEt)_4]^{2-}$ ($-SEt = -SC_2H_5$) (**2**) were prepared from $(t\text{-}Bu_4N)_2[Fe_4S_4Cl_4]$ and $(t\text{-}Bu_4N)_2[Fe_4S_4(SEt)_4]$ solid samples. Solution samples of $[Fe_4S_4Cl_{4-x}(CN)_x]^{2-}$, $[Fe_4S_4Cl_{4-x}(SCN)_x]^{2-}$, and $[Fe_4S_4Cl_{4-x}(OAc)_x]^{2-}$ (OAc = acetate) were prepared by mixing **1** with varying equivalents of $(t\text{-}Bu_4N)CN$, $(t\text{-}Bu_4N)SCN$, and acetic acid, respectively. Solutions of $[Fe_4S_4(SEt)_{4-x}(OPr)_x]^{2-}$ (OPr = propionate) were prepared by mixing **2** with different equivalents of propionic acid. The concentration of the second ligands was tuned to optimize the abundance of a given mixed-ligand species. Solutions of $[Fe_4S_4(SEt)_{4-x}Cl_x]^{2-}$ were prepared by mixing stock solutions **1** and **2** in different molar ratio.

The experiment was carried out with a PES apparatus equipped with an ESI source, a time-of-flight (TOF) mass spectrometer, and a magnetic-bottle TOF photoelectron analyzer.[17] Briefly, the mixed solution samples prepared above were sprayed using a 0.1 mm diameter syringe at a negative bias of −2.2 kV. Anions from the ESI source were guided by a radio frequency quadruple ion guide into a 3D quadruple ion trap, where they were accumulated for 0.1 s, and then were pulsed into the extraction zone of a TOF mass spectrometer.

During PES experiment, the species of interest were selected by a mass gate and decelerated before being intercepted by a probing laser beam in the photodetachment zone of the magnetic-bottle photoelectron analyzer. In the current study, four detachment photon energies were used: 157 nm (7.866 eV) and 193 nm (6.424 eV) from an excimer laser; 266 nm (4.661 eV) and 355 nm (3.496 eV) from a Nd:YAG laser. All experiments were performed at 20 Hz repetition rate with the ion beam off at alternating laser shots for background subtraction. Photoelectrons were collected at nearly 100% efficiency by the magnetic bottle and analyzed in a 4-m long electron flight tube. Photoelectron TOF spectra were collected and then converted to kinetic energy spectra, calibrated by the known spectra of I^- and O^-. The electron binding energy (BE) spectra presented here were obtained by subtracting the kinetic energy (KE) spectra from the detachment photon energies ($h\nu$) (BE = $h\nu$ −

(9) Rao, P. V.; Holm, R. H. *Chem. Rev.* **2004**, *104*, 527−559.
(10) (a) Noodleman, L.; Peng, C. Y.; Case, D. A.; Mouesca, J.-M. *Coord. Chem. Rev.* **1995**, *144*, 199−244. (b) Noodleman, L.; Lovell, T.; Liu, T.; Himo, F.; Torres, R. A. *Curr. Opin. Chem. Biol.* **2002**, *6*, 259−273.
(11) (a) Conover, R. C.; Park, J.-B.; Adams, M. W. W.; Johnson, M. K. *J. Am. Chem. Soc.* **1991**, *113*, 2799−2800. (b) Conover, R. C.; Kowal, A. T.; Fu, W.; Park, J.-B.; Aono, S.; Adams, M. W. W.; Johnson, M. K. *J. Biol. Chem.* **1990**, *265*, 8533−8541. (c) Telser, J.; Smith, E. T.; Adams, M. W. W.; Conover, R. C.; Johnson, M. K.; Hoffman, B. M. *J. Am. Chem. Soc.* **1995**, *117*, 5133−5140.
(12) (a) Calzolai, L.; Gorst, C. M.; Zhao, Z.-H.; Teng, Q.; Adams, M. W. W.; Mar, G. N. L. *Biochemistry* **1995**, *34*, 11373−11384. (b) Busse, S. C.; Mar, G. N. L.; Yu, L. P.; Howard, J. B.; Smith, E. T., Zhao, Z.-H.; Adams, M. W. W. *Biochemistry* **1992**, *31*, 11952−11962. (c) Calzolai, L.; Gorst, C. M.; Bren, K. L.; Zhou, Z.-H.; Adams, M. W. W.; Mar, G. N. L. *J. Am. Chem. Soc.* **1997**, 9341−9350.
(13) (a) Jameson, G. N. L.; Walters, E. M.; Manieri, W.; Schurmann, P.; Johnson, M. K.; Huynh, B. H. *J. Am. Chem. Soc.* **2003**, *125*, 1146−1147. (b) Walsby, C. J.; Ortillo, D.; Broderick, W. E.; Broderick, J. B.; Hoffman, B. M. *J. Am. Chem. Soc.* **2002**, *124*, 11270−11271. (c) Clay, M. D.; Jenney, F. E.; Hagedoorn, P. L.; George, G. N.; Adams, M. W. W.; Johnson, M. K. *J. Am. Chem. Soc.* **2002**, *124*, 788−805. (d) Telser, J.; Huang, H.; Lee, H.-I.; Adams, M. W. W.; Hoffman, B. M. *J. Am. Chem. Soc.* **1998**, *120*, 861−870.
(14) (a) Yoo, S. J.; Angove, H. C.; Burgess, K. K.; Hendrich, M. P.; Munck, E. *J. Am. Chem. Soc.* **1999**, *121*, 2534−2545. (b) Angove, H. C.; Yoo, S. J.; Burgess, B. K.; Munck, E. *J. Am. Chem. Soc.* **1997**, *119*, 8730−8731.
(15) (a) Glaser, T.; Hedman, B.; Hodgson, K. O.; Solomon, E. I. *Acc. Chem. Res.* **2000**, *33*, 859−868. (b) Glaser, T.; Rose, K.; Shadle, S. E.; Hedman, B.; Hodgson, K. O.; Solomon, E. I. *J. Am. Chem. Soc.* **2001**, *123*, 442−454. (c) Anxolabehere-Mallart, E.; Glaser, T.; Frank, P.; Aliverti, A.; Zanetti, G.; Hedman, B.; Hodgson, K. O.; Solomon, E. I. *J. Am. Chem. Soc.* **2001**, *123*, 5444−5452. (d) Rose, K.; Shadle, S. E.; Glaser, T.; de Vries, S.; Cherepanov, A.; Canters, G. W.; Hedman, B.; Hodgson, K. O.; Solomon, E. I. *J. Am. Chem. Soc.* **1999**, *121*, 2353−2363.
(16) (a) Noodleman, L.; Case, D. A. *Adv. Inorg. Chem.* **1992**, 423−470. (b) Noodleman, L.; Baerends, E. J. *J. Am. Che. Soc.* **1984**, *106*, 2316−2327. (c) Noodleman, L.; Case, D. A.; Aizman, A. *J. Am. Chem. Soc.* **1988**, *110*, 1001−1005. (d) Noodleman, L.; Norman, J. G.; Osborne, J. H.; Aizman, A.; Case, D. A. *J. Am. Chem. Soc.* **1985**, *107*, 3418−3426.
(17) Wang, L. S.; Ding, C. F.; Wang, X. B.; Barlow, S. E. *Rev. Sci. Instrum.* **1999**, *70*, 1957.
(18) (a) Yang, X.; Wang, X. B.; Niu, S. Q.; Pickett, C. J.; Ichiye, T.; Wang, L. S. *Phys. Rev. Lett.* **2002**, *89*, 16340−10341. (b) Yang, X.; Wang, X. B.; Wang, L. S. *Int. J. Mass Spectrom.* **2003**, *228*, 797−805.
(19) Wang, X. B.; Niu, S. Q.; Yang, X.; Ibrahim, S. K.; Pickett, C. J.; Ichiye, T.; Wang, L. S. *J. Am. Chem. Soc.* **2003**, *125*, 14072−14081.

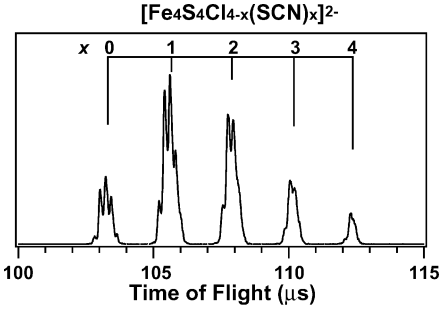

Figure 1. Electrospray mass spectrum of $[Fe_4S_4Cl_{4-x}(SCN)_x]^{2-}$ from reactions of $(t\text{-}Bu_4N)_2[Fe_4S_4Cl_4]$ and $(t\text{-}Bu_4N)SCN$ solutions (1:1 Cl^-/SCN^- molar ratio) in O_2-free acetonitrile.

KE). The energy resolution (ΔKE/KE) was ~2%, i.e., 10 meV for 0.5 eV electrons, as measured from the spectrum of I^- at 355 nm.

3. Experimental Results

3.1. Mass Spectra. Ligand substitution reactions at the terminal positions of the [4Fe-4S] cubane were reported to take place readily.[20−22] However, using conventional purification and characterization methods, it is difficult to obtain pure samples of each of the mixed ligand products from the equilibrium mixture. Here we used ESI to transfer mixed-ligand [4Fe-4S] complexes from the following solution reactions to the gas phase for size-selected PES studies:

$$[Fe_4S_4Cl_4]^{2-} + x\text{CN}^- \rightarrow [Fe_4S_4Cl_{4-x}(\text{CN})_x]^{2-} + x\text{Cl}^- \quad (1)$$

$$[Fe_4S_4Cl_4]^{2-} + x\text{SCN}^- \rightarrow [Fe_4S_4Cl_{4-x}(\text{SCN})_x]^{2-} + x\text{SCN}^- \quad (2)$$

$$[Fe_4S_4Cl_4]^{2-} + x\text{OAc}^- \rightarrow [Fe_4S_4Cl_{4-x}(\text{OAc})_x]^{2-} + x\text{Cl}^- \quad (3)$$

$$[Fe_4S_4(\text{SEt})_4]^{2-} + x\text{OPr}^- \rightarrow [Fe_4S_4(\text{SEt})_{4-x}(\text{OPr})_x]^{2-} + x\text{SEt}^- \quad (4)$$

$$[Fe_4S_4(\text{SEt})_4]^{2-} + [Fe_4S_4Cl_4]^{2-} \rightarrow [Fe_4S_4(\text{SEt})_{4-x}Cl_x]^{2-} + [Fe_4S_4(\text{SEt})_xCl_{4-x}]^{2-} \quad (5)$$

It should be noted that the different products ($x = 0-4$) in the above reactions coexist in equilibrium. Figure 1 shows the ESI mass spectrum of reaction 2 taken with a mixture of $[Fe_4S_4Cl_4]^{2-}$ and SCN^- in 1:1 Cl^-/SCN^- molar ratio. Five $[Fe_4S_4Cl_{4-x}(SCN)_x]^{2-}$ species were observed, ranging from the parent ($x = 0$) to the completely substituted species ($x = 4$). Obvious differences of the isotopic pattern among the five groups of peaks were observed due to the different numbers of Cl^- in each species. Varying the molar ratio of $[Fe_4S_4Cl_4]^{2-}$ and SCN^- in the initial solution changed the relative intensities among the five species. During PES experiments, a given x was optimized by changing the relative concentrations of the initial reactants.

3.2. Photoelectron Spectra. Figures 2−6 show the PES spectra of $[Fe_4S_4Cl_{4-x}(CN)_x]^{2-}$, $[Fe_4S_4Cl_{4-x}(SCN)_x]^{2-}$, $[Fe_4S_4Cl_{4-x}(OAc)_x]^{2-}$, $[Fe_4S_4(SEt)_{4-x}Cl_x]^{2-}$, and $[Fe_4S_4(SEt)_{4-x}(OPr)_x]^{2-}$, respectively, at various photon energies. Overall, the spectra of the mixed-ligand complexes are similar to those of the precursor complexes $[Fe_4S_4(SEt)_4]^{2-}$ and $[Fe_4S_4Cl_4]^{2-}$, which were reported previously,[18] and are shown here for comparisons. All the spectra exhibit a weak but well-defined threshold feature X in the lower binding energy range, followed by an intense and well-defined band (A) and continuous spectral transitions at high binding energies. In each series, the electron binding energies of $[Fe_4S_4(L_1)_{4-x}(L_2)_x]^{2-}$ change systematically with the substitution number. Significant spectral cutoff was observed in all the PES spectra due to the repulsive Coulomb barrier (RCB) present in multiply charged anions,[23] as will be discussed below.

3.2.1. PES Spectra of $[Fe_4S_4Cl_{4-x}(CN)_x]^{2-}$. The PES spectra of $[Fe_4S_4Cl_{4-x}(CN)_x]^{2-}$ ($x = 0-4$) are shown in Figure 2 at 157, 193, and 266 nm. All the spectra have similar spectral features, which rigidly shift to higher binding energies with increasing numbers of the CN^- ligand. In the 157 nm spectra (Figure 2a), the broad and intense feature in the high binding energy range due to the Cl^- terminal ligands was clearly observed. The intensity of the Cl^- feature decreased with increasing substitution, accompanied by the appearance of a new feature due to CN^- at even higher binding energies. At $x = 4$, the band due to Cl^- disappeared completely and the feature from CN^- was dominant. At 193 nm (Figure 2b), the CN^- features disappeared due to the RCB, whereas the X and A bands were better resolved. At 266 nm, all the higher binding energy features were cut off by the RCB and only the two lowest binding energy bands (X and A) were observed intact.

3.2.2. PES Spectra of $[Fe_4S_4Cl_{4-x}(SCN)_x]^{2-}$. The PES spectra of the $[Fe_4S_4Cl_{4-x}(SCN)_x]^{2-}$ series are shown in Figure 3 at 193, 266, and 355 nm. The spectra of the mixed-ligand species are again similar to that of the parent, except that the binding energies increased with x and the SCN^- ligand gave a very prominent PES feature even at $x = 1$ in the 193 nm spectra (Figure 3a). Despite the fact that the binding energies of the SCN^- features were lower than that of Cl^-, the SCN^- ligands seemed to induce a much larger increase of binding energies in the $[Fe_4S_4Cl_{4-x}(SCN)_x]^{2-}$ complexes. In fact, the 1.84 eV ADE of $[Fe_4S_4(SCN)_4]^{2-}$ is the highest among all the $[Fe_4S_4L_4]^{2-}$ cubane complexes that we have examined. In the 266 nm spectra (Figure 3b), high binding energy features including that due to SCN^- were mostly cut off by the RCB. At 355 nm, only the X band was well observed (Figure 3c), though for $x = 3$ the electron signals became much weaker and the peak position shifted

(20) (a) Cleland, W. E.; Holtman, D. A.; Sabat, M.; Ibers, J. A.; DeFotis, G. C.; Averill, B. A. *J. Am. Chem. Soc.* **1983**, *105*, 6021−6031. (b) Wong, G. B.; Bobrik, M. A.; Holm, R. H. *Inorg. Chem.* **1978**, *17*, 578−584. (c) Que, L.; Bobrik, M. A.; Ibers, J. A.; Holm, R. H. *J. Am. Chem. Soc.* **1974**, *96*, 4168−5344.

(21) (a) Que, L.; Anglin, J. R.; Bobrik, M. A.; Davison, A.; Holm, R. H. *J. Am. Chem. Soc.* **1974**, *96*, 6042−6048. (b) DePamphilis, B. V.; Averill, B. A.; Herskovitz, T.; Que, L.; Holm, R. H. *J. Am. Chem. Soc.* **1974**, *96*, 4159−4167.

(22) Ohno, R.; Ueyama, N.; Nakamura, A. *Inorg. Chem.* **1991**, *30*, 4887−4891.

(23) (a) Wang, L. S.; Ding, C. F.; Wang, X. B.; Nicholas, J. B. *Phys. Rev. Lett.* **1998**, *81*, 2667. (b) Wang, X. B.; Ding, C. F.; Wang, L. S. *Phys. Rev. Lett.* **1998**, *81*, 3351−3354. (c) Wang, X. B.; Wang, L. S. *Nature (London)* **1999**, *400*, 245−248. (d) Wang, L. S.; Wang, X. B. *J. Phys. Chem. A* **2000**, *104*, 1978−1990.

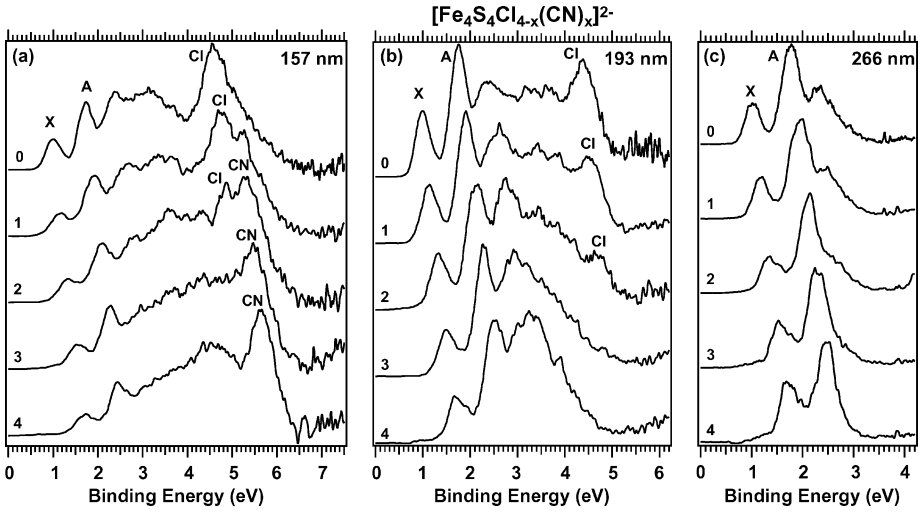

Figure 2. Photoelectron spectra of ligand substitution series $[Fe_4S_4Cl_{4-x}(CN)_x]^{2-}$ ($x = 0-4$) at (a) 157 nm (7.866 eV), (b) 193 nm (6.424 eV), and (c) 266 nm (4.661 eV).

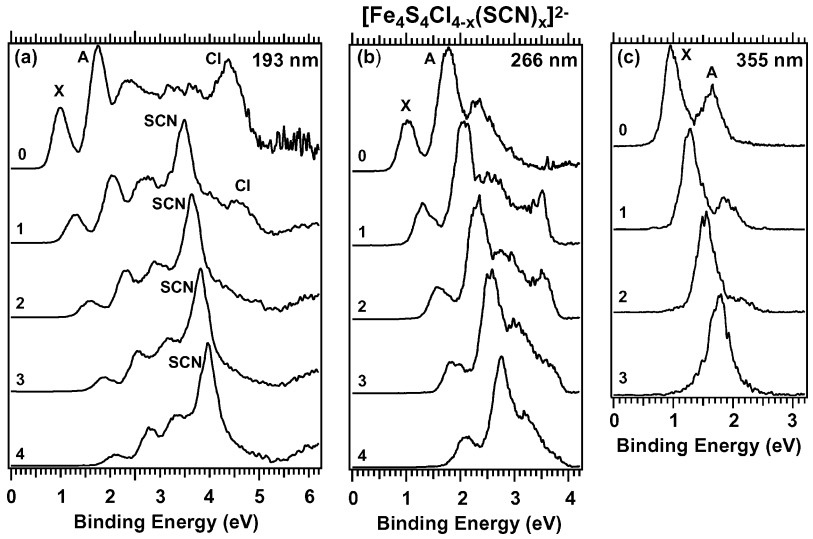

Figure 3. Photoelectron spectra of ligand substitution series $[Fe_4S_4Cl_{4-x}(SCN)_x]^{2-}$ ($x = 0-4$) at (a) 193 nm, (b) 266 nm, and (c) 355 nm (3.496 eV).

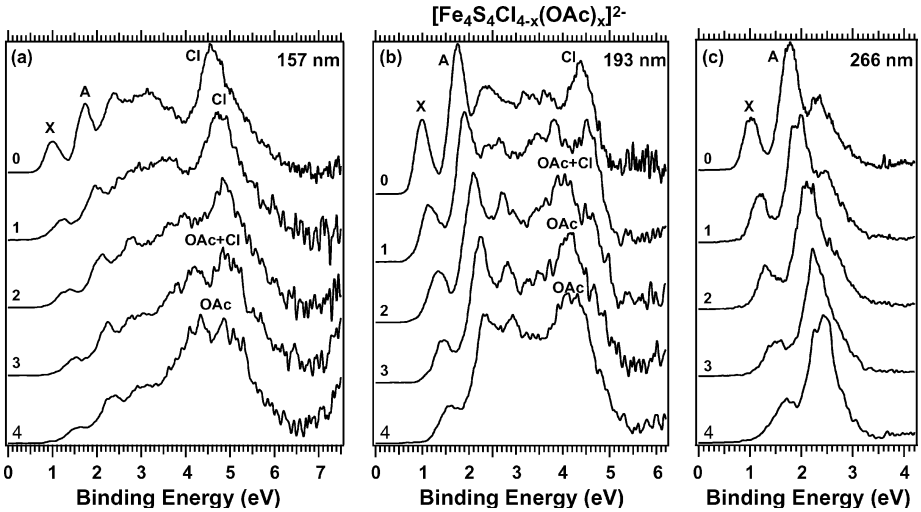

Figure 4. Photoelectron spectra of ligand substitution series $[Fe_4S_4Cl_{4-x}(OAc)_x]^{2-}$ ($x = 0-4$) at (a) 157 nm, (b) 193 nm, and (c) 266 nm.

from 1.88 eV in the 266 nm spectrum to 1.72 eV in the 355 nm spectrum, as a result of electron tunneling effect caused by the RCB.[23,24] No electron signals could be detected for $[Fe_4S_4(SCN)_4]^{2-}$ at 355 nm, suggesting this photon energy was below the barrier height of the RCB associated with the ground-state transition.

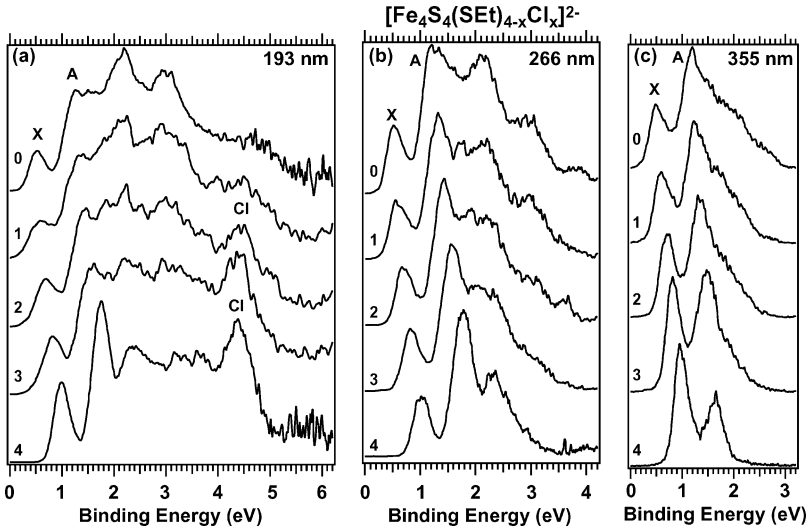

Figure 5. Photoelectron spectra of ligand substitution series $[Fe_4S_4(SEt)_{4-x}Cl_x]^{2-}$ ($x = 0-4$) at (a) 193 nm, (b) 266 nm, and (c) 355 nm.

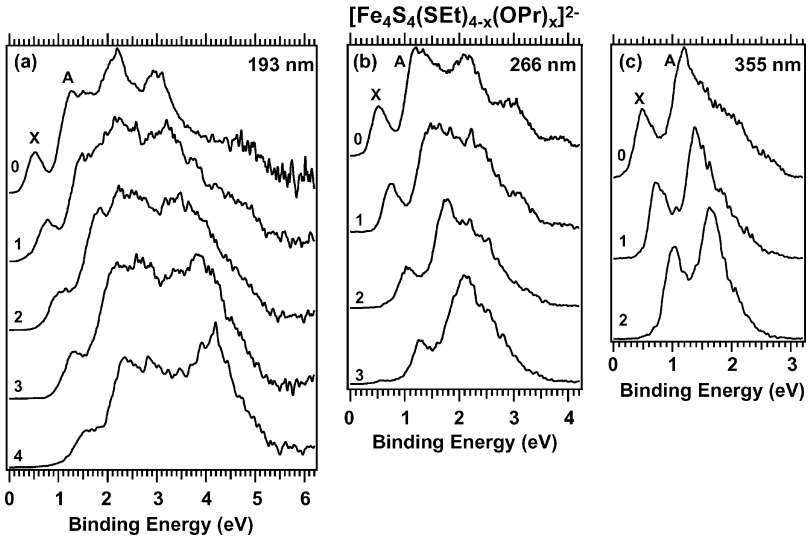

Figure 6. Photoelectron spectra of ligand substitution series $[Fe_4S_4(SEt)_{4-x}(OPr)_x]^{2-}$ ($x = 0-4$) at (a) 193 nm, (b) 266 nm, and (c) 355 nm.

3.2.3. PES Spectra of $[Fe_4S_4Cl_{4-x}(OAc)_x]^{2-}$. The PES spectra for this series are shown in Figure 4 at 157, 193, and 266 nm. The spectra of the mixed-ligand species are again similar to the parent, and their binding energies also increase with *x*. However, the threshold band X, as well as the band A, seemed to be broader, in particular, for that of $x = 4$. The features due to the substituent ligand (OAc^-) (Figure 4a) were not as prominent as those observed for CN^- or SCN^- in their respective mixed-ligand spectra primarily because the binding energies of the OAc^- ligand features were similar to that of Cl^- and they overlapped. The 157 nm spectra for the $x = 3$ and 4 species (Figure 4a) showed that the OAc^- ligands gave rise to two broad features at similar binding energies as expected for Cl^-. At 193 nm (Figure 4b), again there was significant cut off at the high binding energy side due to the RCB. The bands due to OAc^- became more prominent in the 193 nm spectra, since the Cl^- features were more severely influenced by the RCB. The higher binding energy part of the OAc^- bands was also cut off by the RCB, but the lower binding energy component was still prominent. At 266 nm (Figure 4c), again most of the higher binding energy bands were cut off due to the RCB and only the X and A bands were well observed. We note that the 266 nm spectra of $[Fe_4S_4Cl_{4-x}(OAc)_x]^{2-}$ are nearly identical with those of $[Fe_4S_4Cl_{4-x}(CN)_x]^{2-}$ (Figure 2c) because they have similar electron binding energies and similar RCBs.

3.2.4. PES Spectra of $[Fe_4S_4(SEt)_{4-x}Cl_x]^{2-}$. The spectra of $[Fe_4S_4(SEt)_{4-x}Cl_x]^{2-}$ are shown in Figure 5 at 157, 193, and 266 nm. As expected, the binding energies increase with the number of Cl^- ligands. In the 193 nm spectra (Figure 5a), the Cl^- feature emerged gradually with the increase of substitution number *x*. The 266 and 355 nm spectra were better resolved, while more and more higher binding energy features were cut off by the RCB.

3.2.5. PES Spectra of $[Fe_4S_4(SEt)_{4-x}(OPr)_x]^{2-}$. The spectra of this series are shown in Figure 6 at 193, 266, and 355 nm. Here the OPr^- substituent ligand was used instead of the smaller OAc^- ligand as in $[Fe_4S_4Cl_{4-x}(OAc)_x]^{2-}$ because OAc^- (mass = 59) has a nearly identical mass as

(24) Wang, X. B.; Ding, C. F.; Wang, L. S. *Chem. Phys. Lett.* **1999**, *307*, 391−396.

Table 1. Adiabatic (ADE) and Vertical (VDE) Electron-Binding Energies for the X and A Bands, the Separation between the X−A Bands ($\Delta_{(A-X)}$), and the Bandwidth of the X Band (λ_{oxd}) from the Photoelectron Spectra of $[Fe_4S_4(L_1)_{4-x}(L_2)_x]^{2-}$ (All Energies in eV)

	ADE	VDE(X)	VDE(A)	$\Delta_{(A-X)}$	λ_{oxd}
$[Fe_4S_4Cl_4]^{2-}$	0.80(8)	1.01(6)	1.78(6)	0.77	0.21
$[Fe_4S_4Cl_3(CN)]^{2-}$	0.97(8)	1.17(6)	2.00(6)	0.83	0.20
$[Fe_4S_4Cl_2(CN)_2]^{2-}$	1.09(10)	1.36(8)	2.15(4)	0.79	0.27
$[Fe_4S_4Cl(CN)_3]^{2-}$	1.27(8)	1.53(6)	2.30(6)	0.77	0.26
$[Fe_4S_4(CN)_4]^{2-}$	1.47(11)	1.69(6)	2.46(6)	0.77	0.22
$[Fe_4S_4Cl_3(SCN)]^{2-}$	1.06(8)	1.30(5)	2.07(7)	0.77	0.24
$[Fe_4S_4Cl_2(SCN)_2]^{2-}$	1.36(9)	1.61(5)	2.31(5)	0.70	0.25
$[Fe_4S_4Cl(SCN)_3]^{2-}$	1.61(10)	1.88(10)	2.55(6)	0.67	0.27
$[Fe_4S_4(SCN)_4]^{2-}$	1.84(10)	2.10(8)	2.76(5)	0.66	0.26
$[Fe_4S_4Cl_3(OAc)]^{2-}$	0.93(9)	1.19(7)	1.92(8)	0.73	0.26
$[Fe_4S_4Cl_2(OAc)_2]^{2-}$	1.04(9)	1.29(6)	2.10(8)	0.81	0.25
$[Fe_4S_4Cl(OAc)_3]^{2-}$	1.11(12)	1.48(10)	2.22(6)	0.74	0.37
$[Fe_4S_4(OAc)_4]^{2-}$	1.18(12)	1.72(8)	2.40(10)	0.68	0.54
$[Fe_4S_4(SEt)_4]^{2-}$	0.29(8)	0.52(6)	1.20(6)	0.68	0.23
$[Fe_4S_4(SEt)_3Cl]^{2-}$	0.41(6)	0.60(8)	1.33(6)	0.73	0.19
$[Fe_4S_4(SEt)_2Cl_2]^{2-}$	0.52(8)	0.71(6)	1.43(5)	0.72	0.19
$[Fe_4S_4(SEt)Cl_3]^{2-}$	0.62(8)	0.82(6)	1.56(6)	0.74	0.20
$[Fe_4S_4(SEt)_3(OPr)]^{2-}$	0.57(8)	0.75(6)	1.47(8)	0.72	0.18
$[Fe_4S_4(SEt)_2(OPr)_2]^{2-}$	0.78(10)	1.03 (8)	1.75(6)	0.72	0.25
$[Fe_4S_4(SEt)(OPr)_3]^{2-}$	1.01(10)	1.32(6)	2.08(8)	0.76	0.31
$[Fe_4S_4(OPr)_4]^{2-}$	1.22(12)	1.56(12)	2.34(8)	0.78	0.34

SEt^- (mss = 61) and would make it very difficult to separate the mixed-ligand $[Fe_4S_4(SEt)_{4-x}(OAc)_x]^{2-}$ species from the parent $[Fe_4S_4(SEt)_4]^{2-}$. OPr^- ($CH_3CH_2CO_2^-$) should have the same coordination and influence to the cubane as OAc^- ($CH_3CO_2^-$). Indeed, the PES spectrum of $[Fe_4S_4(OPr)_4]^{2-}$ (Figure 6a) is identical with that of $[Fe_4S_4(OAc)_4]^{2-}$ (Figure 4b). We observed that substitution of SEt^- with OPr^- systematically increased the electron binding energies of the mixed-ligand $[Fe_4S_4(SEt)_{4-x}(OPr)_x]^{2-}$ species, which all gave similar PES spectral features. The VDE of the X band was observed to increase from 0.52 to 1.65 eV from $x = 0$ to 4. Because of reduced mass intensities for higher substitution numbers in the $[Fe_4S_4(SEt)_{4-x}(OPr)_x]^{2-}$ series, PES spectra were only measured up to $x = 3$ at 266 nm (Figure 6b) and up to $x = 2$ at 355 nm (Figure 6c). Again cutoff of high binding energy features due to the RCB was observed in each lower photon energy spectrum. The width of the X band increased in the OPr^--ligated species and seemed to increase with x, becoming substantially broad in the spectrum of the $x = 4$ species, similar to that observed for the OAc^--substituted species (Figure 4).

3.2.6. ADEs and VDEs. The ADE and VDE of the threshold band (X) and the VDE of the second detachment band (A) for all the species are given in Table 1. Due to the lack of vibrational resolution, the ADEs were measured by drawing a straight line along the leading edge of the threshold band and then adding a constant to the intersection with the binding energy axis to take into account the instrumental resolution at the given energy range. This procedure was rather approximate, but consistent data were obtained from the spectra taken at different photon energies. The ADEs reported in Table 1 were determined from the lowest photon energy spectrum available for each complex because of the better resolution at lower photon energies. The VDE was measured straightforwardly from the peak maximum. The X bandwidth was also given in Table 1 as λ_{oxd} calculated by [VDE(X) − ADE]. In general, the X bandwidth did not vary significantly for the different species, except for the carboxylate-coordinated systems, in particular, $[Fe_4S_4(OAc)_4]^{2-}$ and $[Fe_4S_4(OPr)_4]^{2-}$.

4. Discussion

4.1. Intramolecular Coulomb Repulsion and the Repulsive Coulomb Barrier. All the [4Fe-4S] complexes presented in this study are doubly charged and have a strong intramolecular electrostatic repulsion. As shown previously,[23] the short-range attraction and long-range Coulomb repulsion for an outgoing electron create a potential barrier, called repulsive Coulomb barrier, which has profound effects on the PES spectra of multiply charged anions,[23,24] as discussed above in comparing the spectra at different photon energies. The RCB prevents electrons with low kinetic energies from being emitted, causing the cutoff at the higher binding energy side (note that BE = $h\nu$ − KE) observed in all the PES spectra in Figures 2−6. RCB is an important physical property of a free multiply charged anion and can be estimated from the spectral cutoff and by comparing PES spectra measured at different photon energies.[23] We reported previously the RCB for $[Fe_4S_4Cl_4]^{2-}$ and $[Fe_4S_4(SEt)_4]^{2-}$ to be 2.0 and 1.6 eV, respectively.[19] From the data presented in Figures 2−4, we estimated the RCB for $[Fe_4S_4(CN)_4]^{2-}$, $[Fe_4S_4(SCN)_4]^{2-}$, and $[Fe_4S_4(OAc)_4]^{2-}$ to be 2.0, 1.4, and 1.9 eV, respectively. These were approximate values. But they are consistent with the expectation that in general the RCB depends on the size of the multiply charged anions or the separation between the excess charges.[23] The RCB for $[Fe_4S_4(OPr)_4]^{2-}$ could not be estimated because only the 193 nm data were able to be measured, but it was expected to be the same as that of $[Fe_4S_4(OAc)_4]^{2-}$. RCBs for the mixed-ligand complexes were not estimated because of the uncertainty in the evaluation procedure. They were expected to fall between those of the two parents ($x = 0$ and $x = 4$).

4.2. Redox Reorganization Energy. The threshold feature X in the PES spectrum corresponds to removing an electron from the HOMO of each species. The ADE of the X band represents the gas-phase oxidation potential. The width of

the X band reflects the geometry changes after one electron is transferred and hence is related to the intrinsic reorganization energy (λ_{oxd}) upon oxidation.[25] As shown previously,[19] the values of λ_{oxd} can be obtained from the difference between VDE and ADE of the X band, as given in Table 1. The λ_{oxd} values are almost identical for all the species, ranging from 0.20 to 0.25 eV, except for the two fully carboxylate-coordinated complexes. These values are also similar to our previous report on [Fe$_4$S$_4$L$_4$]$^{2-}$ with L = −SH, −SEt, −Cl, −Br, and −I. The nearly constant reorganization energy indicates the stability of the cubane core with respect to the terminal ligands. It is particularly surprising that even the mixed-ligand species did not give rise to a substantially broader X band. Only [Fe$_4$S$_4$(OAc)$_4$]$^{2-}$ and [Fe$_4$S$_4$(OPr)$_4$]$^{2-}$ gave a much broader X band, suggesting a much larger geometry change upon removing an electron from the HOMO of the two fully carboxylate-coordinated cubanes. Preliminary theoretical calculations indicated that structural isomers may exist with the carboxylate coordinated cubanes (Shuqiang Niu, private communications), which could be an alternative explanation for the broad X band in these species.

4.3. Electronic Structure of the Mixed-Ligand Cubane. Our recent PES work on a series of cubane analogue complexes, [Fe$_4$S$_4$L$_4$]$^{2-}$ with L = −SH, −SEt, −Cl, −Br, and −I, as well as the Se-substituted cubane complexes,[19] confirmed the two-layer "inverted level scheme" based on the broken symmetry DFT calculations for the electronic structure of the cubanes.[10,16] In the mixed-ligand complexes, [Fe$_4$S$_4$(L$_1$)$_x$(L$_2$)$_{4-x}$]$^{2-}$, because of the asymmetry induced by the two different ligands, L$_1$ and L$_2$, it was not clear if the two-layer "inverted level" scheme would still be applicable. The asymmetry of the ligand environment makes the two sublayers nonequivalent and can cause an energetic shift of the two sublayers, as schematically shown in Figure 7. This shift should be reflected in the width of the X band, which is due to removal of the two minority electrons.

Our PES spectra (Figures 2−6) showed that all the mixed-ligand cubanes gave spectral features nearly identical with those of the parents except for the systematic increase in binding energies and the additional ligand-induced bands at higher binding energies. In particular, the spectral features in the lower binding energy side were almost identical in all the cubane complexes. Even the separation between the X and A bands was nearly identical in all the spectra, as shown in Table 1. The fact that the X bandwidth is also nearly identical suggested that the asymmetry of the coordination environment in the mixed-ligand cubane was not significant enough to change the relative energies of the two layers. These observations suggested that while the electron binding energies (oxidation potentials) of the cubane complexes are very sensitive to the terminal ligands, the electronic structures entailed in the two-layer "inverted level scheme" are not sensitive to the terminal ligand environment, further evidence for the robustness of the cubane as a structural and functional unit.

(25) Wang, X. B.; Wang, L. S. *J. Chem. Phys.* **2000**, *112*, 6959−6962. Amashukeli, X.; Winkler, J. R.; Gray, H. B.; Gruhn, N. E.; Lichtenberger, D. L. *J. Phys. Chem. A* **2002**, *106*, 7593−7598.

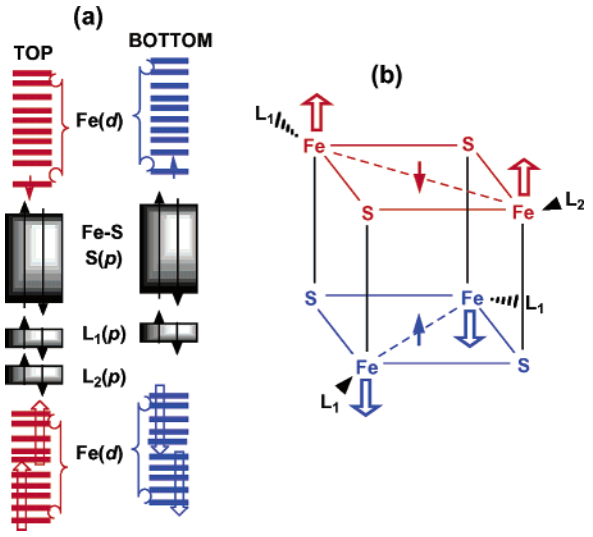

Figure 7. (a) Schematic "inverted level scheme" for a mixed-ligand cubane [Fe$_4$S$_4$(L$_1$)$_3$(L$_2$)]$^{2-}$. (b) Two-layer model showing the spin-coupling in the [4Fe-4S]$^{2+}$ cubane core. The large arrows represent the d^5 majority-spin electrons on each Fe, and the small arrows represent a single minority-spin electron delocalized over two Fe centers in each layer.

4.4. Influence of the Terminal Ligands on the Intrinsic Redox Properties of the Cubane. Although the terminal ligands do not seem to change the electronic structures of the cubane significantly, they do have dramatic effects on the electron binding energies of the cubane, which are related to the intrinsic redox properties of the cubane complexes. Our previous study showed that the electron-binding energies of the cubane are strongly dependent on the terminal ligands and are related to the electron-donating or -withdrawing capability of the terminal ligands.[19] The HOMO of the [Fe$_4$S$_4$L$_4$]$^{2-}$ complex consists of Fe−Fe bonding and Fe−L antibonding interactions. Strong electron donors, such as SEt$^-$ and SH$^-$, destabilize the HOMO, resulting in much lower electron binding energies, whereas the halogen ligands are strong electron-withdrawing ligands and their cubane complexes all have rather high electron-binding energies. The same trend was observed in the current study, both CN$^-$ and SCN$^-$ are strong electron-withdrawing ligands and they significantly increase the electron-binding energies of the cubane complexes.

4.4.1. Observation of Linear Relations of Binding Energies vs *x* in Fe$_4$S$_4$(L$_1$)$_{4-x}$(L$_2$)$_x$]$^{2-}$. An interesting observation in this study is the linear relationship between the electron-binding energies and the substitution number (x) in the mixed-ligand cubanes, as shown in Figure 8, where the ADE and the VDE of both the X and A bands are plotted against the substitution number x. We found that the binding energy of the mixed-ligand complex, [Fe$_4$S$_4$(L$_1$)$_{4-x}$(L$_2$)$_x$]$^{2-}$, can be expressed as

$$BE = BE_1 + \gamma x \qquad (6)$$

where BE$_1$ is the binding energy of [Fe$_4$S$_4$(L$_1$)$_4$]$^{2-}$ ($x = 0$) and γ is the slope.

The linear relationship suggests that each of the four terminal ligands contribute to the total binding energy of the cubane complex independently and additively. Therefore, the

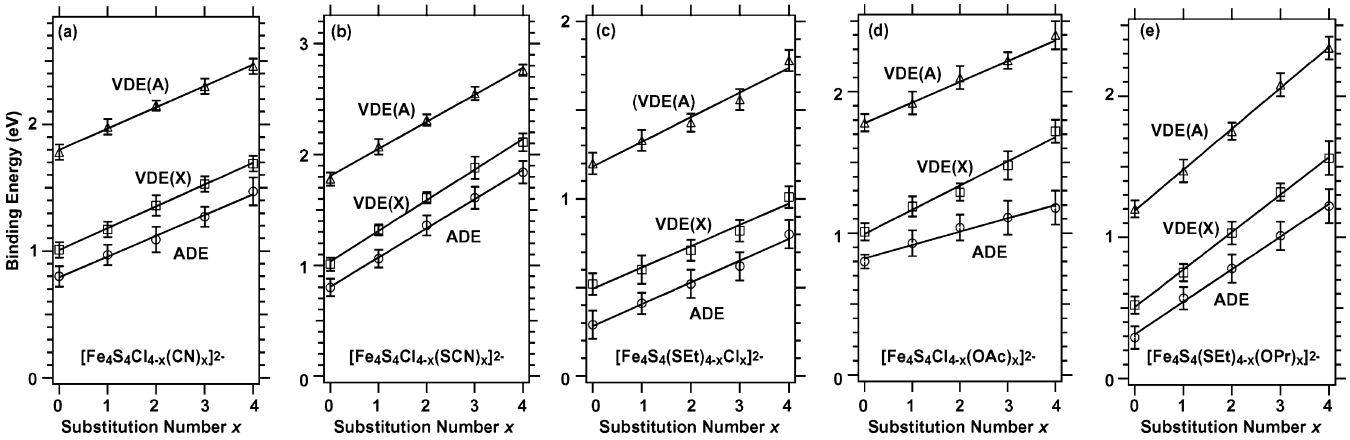

Figure 8. Linear relationships of binding energies [ADE, VDE(X), VDE(A)] with substitution number x: (a) $[Fe_4S_4Cl_{4-x}(CN)_x]^{2-}$; (b) $[Fe_4S_4Cl_{4-x}(SCN)_x]^{2-}$; (c) $[Fe_4S_4(SEt)_{4-x}Cl_x]^{2-}$; (d) $[Fe_4S_4Cl_{4-x}(OAc)_x]^{2-}$; (e) $[Fe_4S_4(SEt)_{4-x}(OPr)_x]^{2-}$. The solid lines are from linear fittings.

BE can be written as

$$BE = BE_0 + (4 - x)\delta_1 + x\delta_2 \quad (7)$$

where BE_0 is the electron-binding energy of the bare cubane core $[Fe_4S_4]^{2+}$ and δ_1 and δ_2 are contributions to the binding energy from ligands L_1 and L_2, respectively. Equation 7 can be rearranged as

$$BE = BE_0 + 4\delta_1 + x(\delta_2 - \delta_1) \quad (8)$$

Comparing eqs 6 and 8, we see that the slope γ equals to $(\delta_2 - \delta_1)$, i.e., the difference of the contributions to the binding energy by ligands L_2 and L_1.

We obtained the following slopes from Figure 8: $\delta_{CN^-} - \delta_{Cl^-} = 0.16$ eV, $\delta_{SCN^-} - \delta_{Cl^-} = 0.26$ eV, $\delta_{Cl^-} - \delta_{SEt^-} = 0.13$ eV, $\delta_{OAc^-} - \delta_{Cl^-} = 0.15$ eV, and $\delta_{OPr^-} - \delta_{SEt^-} = 0.27$ eV for both the VDE(X) and VDE(A) curves. The same slope was found for the ADE curves of the CN^-/Cl^-, SCN^-/Cl^-, and SEt^-/Cl^- systems as the VDE curves. But the ADE curves for the OAc^-/Cl^- and OPr^-/SEt^- systems gave different slopes from the VDE curves, $\delta_{OAc^-} - \delta_{Cl^-} = 0.10$ eV and $\delta_{OPr^-} - \delta_{SEt^-} = 0.22$ eV, as can be seen clearly from Figure 8d,e. This was caused by the broadening of the X band in the carboxylate-coordinated complexes.

Thus, if the binding energies of two cubane complexes, $[Fe_4S_4(L_1)_4]^{2-}$ and $[Fe_4S_4(L_2)_4]^{2-}$, are known, one can predict the binding energies of the L_1/L_2 mixed-ligand complexes, $[Fe_4S_4(L_1)_{4-x}(L_2)_x]^{2-}$, because the slope can be calculated: $\delta_2 - \delta_1 = (BE_2 - BE_1)/4$. For example, from the known VDEs for $[Fe_4S_4Cl_4]^{2-}$ (1.00 eV) and $[Fe_4S_4I_4]^{2-}$ (1.66 eV), we can predict the VDEs for the three mixed-ligand complexes, $[Fe_4S_4Cl_3I]^{2-}$, $[Fe_4S_4Cl_2I_2]^{2-}$, and $[Fe_4S_4ClI_3]^{2-}$, to be 1.16, 1.33, and 1.49 eV, respectively. These predicted values are indeed in good agreement with our experimental measurements (not shown).

4.4.2. Comparison with Redox Potentials of Mixed-Ligand Cubanes in Solution. Redox potentials are known for many cubane complexes with four identical ligands.[21,22,26] Redox potentials for some mixed-ligand complexes are also known.[27] For example, ligand substitution reactions between $[Fe_4S_4(SCH_2Ph)_4]^{2-}$ and CH_3COCl and $(CH_3CO)_2O$ were studied to give two series of mixed-ligand substitution species, $[Fe_4S_4(SCH_2Ph)_{4-x}Cl_x]^{2-}$ and $[Fe_4S_4(SCH_2Ph)_{4-x}(OAc)_x]^{2-}$ with $x = 1-4$.[27] It was found that each substitution by Cl^- or OAc^- induced a positive reduction potential shift by about 100 meV; i.e., a linear relationship between the reduction potentials and x was observed in the two mixed-ligand complexes. This observation is very similar to our observation in the gas phase for the electron binding energies (oxidation potentials) of the mixed-ligand cubane complexes. The solution results concerned a reduction of a 2− cubane to a 3− cubane, which involved addition of an electron to the LUMO of the 2− cubane complexes, whereas the gas-phase data were about the oxidation of 2− cubanes to 1−, which involved removal of an electron from the HOMO. However, as our PES results have shown, all the molecular orbitals of the cubane complexes rigidly shift with the terminal ligands. We expect that the LUMO of the cubane should shift accordingly. Thus, similar linear behaviors between our gas phase data and the solution phase redox potentials suggest that our gas-phase data can be reliably used to extrapolate to behaviors in solution for the mixed-ligand complexes. These results give the intrinsic redox potentials of the cubane complexes and provide an experimental basis to partition the intrinsic and extrinsic factors to the redox potentials in solution.

The independent contribution of ligand toward the redox potentials of transition metal complexes, i.e., the "ligand additivity" model, has been well documented in inorganic chemistry, albeit mostly for mononuclear redox species.[28] The "ligand additivity" toward the redox potential of the [4Fe-4S] complexes confirms further the robustness of the [4Fe-4S] cubane as a structural and functional unit. It shows

(26) (a) Holm, R. H. *Adv. Inorg. Chem.* **1992**, *38*, 1−72. (b) Zhou, C.; Holm, R. H. *Inorg. Chem.* **1997**, *36*, 4066−4077. (c) Zhou, J.; Raebiger, J. W.; Crawford, C. A.; Holm, R. H. *J. Am. Che. Soc.* **1997**, *119*, 6242−6250. (d) Zhou, J.; Hu, Z.; Munck, E.; Holm, R. H. *J. Am. Chem. Soc.* **1996**, *118*, 1966−1980. (e) Ciurli, S.; Carrie, M.; Weigel, J. A.; Carney, M. J.; Stack, T. D. P.; Papaefthymiou, G. C.; Holm, R. H. *J. Am. Chem. Soc.* **1990**, *112*, 2654−2664.

(27) Johnson, R. W.; Holm, R. H *J. Am. Chem. Soc*. **1978**, *100*, 5338−5344.

(28) (a) Treichel, P. M.; Durren, G. E.; Mueh, H. J. *J. Organomet. Chem*. **1972**, *44*, 339−344. (b) Pickett, C. J.; Pletcher, D. J. *J. Organomet. Chem*. **1975**, *102*, 327−333. (c) Sarapu, A.; Fenske, R. F. *Inorg. Chem*. **1975**, *14*, 247−253. (d) Lever, A. B. P. *Inorg. Chem.* **1990**, *29*, 1271−1285.

that the terminal ligands act as perturbations on the electronic structure of the cubane.

5. Conclusions

Using electrospray and photoelectron spectroscopy, we were able to select species from an equilibrium solution of mixed cubane complexes, $[Fe_4S_4(L_1)_{4-x}(L_2)_x]^{2-}$, and study their electronic structures in the gas phase in a ligand-specific fashion. This technique avoided the influence of the solvation effects so that the changes of the intrinsic electronic structure due to sequential substitution and asymmetric terminal ligand coordination were studied systematically. PES data were reported for five mixed-ligand series, $[Fe_4S_4Cl_{4-x}(CN)_x]^{2-}$, $[Fe_4S_4Cl_{4-x}(SCN)_x]^{2-}$, $[Fe_4S_4Cl_{4-x}(OAc)_x]^{2-}$, $[Fe_4S_4(SEt)_{4-x}Cl_x]^{2-}$, and $[Fe_4S_4(SEt)_{4-x}(OPr)_x]^{2-}$ ($x = 0-4$). The PES spectra showed that the electronic structure of the mixed-ligand species also conforms to the "inverted level scheme" and the asymmetric coordination environment has no major influence on the electronic structure of the cubane. However, significant and systematic changes in electron-binding energies were observed with each substitution of the terminal ligand and the electron-binding energies increase in the order $SEt^- \rightarrow Cl^- \rightarrow OAc^- \sim OPr^- \rightarrow CN^- \rightarrow SCN^-$, consistent with the electron-withdrawing capability of each ligand type. A linear relationship was observed for each mixed-ligand system between the electron-binding energies and the substitution number, suggesting that the contribution of each ligand toward the electron-binding energy of the cubane is independent and additive. This observation was consistent with previous observations of redox potentials in solution of mixed-ligand cubanes. The linear relationship reveals the electrostatic nature of the interaction between the cubane and the terminal ligands and validates the approach to partition the extrinsic contributions to the cubane redox potentials due to different environmental factors.

Acknowledgment. Valuable discussions with Prof. T. Ichiye and Dr. Shuqiang Niu and support for this research by the National Institutes of Health (Grant GM-63555) are gratefully acknowledged. We thank Dr. C. Zhou from Prof. R. H. Holm's group for providing us the initial (t-Bu$_4$N)$_2$[Fe$_4$S$_4$Cl$_4$] and (t-Bu$_4$N)$_2$[Fe$_4$S$_4$(SEt)$_4$] samples. The experimental work was performed at the W. R. Wiley Environmental Molecular Sciences Laboratory, a national scientific user facility sponsored by DOE's Office of Biological and Environmental Research and located at Pacific Northwest National Laboratory, which is operated for DOE by Battelle.

IC0495261